



HAL
open science

Darcy's law of yield stress fluids on a treelike network

Vincenzo Maria Schimmenti, Federico Lanza, Alex Hansen, Silvio Franz,
Alberto Rosso, Laurent Talon, Andrea de Luca

► **To cite this version:**

Vincenzo Maria Schimmenti, Federico Lanza, Alex Hansen, Silvio Franz, Alberto Rosso, et al.. Darcy's law of yield stress fluids on a treelike network. *Physical Review E*, 2023, 108 (2), pp.L023102. 10.1103/PhysRevE.108.L023102 . hal-04262567

HAL Id: hal-04262567

<https://hal.science/hal-04262567>

Submitted on 5 Dec 2023

HAL is a multi-disciplinary open access archive for the deposit and dissemination of scientific research documents, whether they are published or not. The documents may come from teaching and research institutions in France or abroad, or from public or private research centers.

L'archive ouverte pluridisciplinaire **HAL**, est destinée au dépôt et à la diffusion de documents scientifiques de niveau recherche, publiés ou non, émanant des établissements d'enseignement et de recherche français ou étrangers, des laboratoires publics ou privés.

The Darcy's law of yield stress fluids on a tree-like network

Vincenzo Maria Schimmenti,¹ Federico Lanza,^{1,2} Alex Hansen,²
 Silvio Franz,¹ Alberto Rosso,¹ Laurent Talon,³ and Andrea De Luca⁴

¹Université Paris-Saclay, CNRS, LPTMS, 91405, Orsay, France

²PoreLab, Department of Physics,

Norwegian University of Science and Technology, N-7491, Trondheim, Norway

³Université Paris-Saclay, CNRS, FAST, 91405, Orsay, France

⁴Laboratoire de Physique Théorique et Modélisation, CY Cergy Paris Université,
 CNRS, F-95302 Cergy-Pontoise, France

(Dated: November 28, 2022)

Understanding the flow of yield stress fluids in porous media is a major challenge. In particular, experiments and extensive numerical simulations report a non-linear Darcy's law as a function of the pressure gradient. In this letter, we consider a tree-like porous structure for which the problem of the flow can be resolved exactly thanks to a mapping with the directed polymer (DP) with disordered bond energies on the Cayley tree. Our results confirm the non-linear behavior of the flow and expresses its full pressure-dependence via the density of low-energy states of DP restricted to vanishing overlap. These universal predictions are confirmed by extensive numerical simulations.

In a series of experiments during the nineteenth century, Henry Darcy studied the flow of water in a cylinder filled with sand [1] and established the empirical law for the flow rate Q as a function of the pressure difference P between the two ends of the cylinder

$$Q = \kappa R^2 P / (\eta L) \quad (1)$$

here R and L are respectively the radius and the length of the cylinder, η is the viscosity of the fluid and κ is the permeability of the medium. Darcy gave an interpretation to the permeability κ starting from the Poiseuille's law which holds for empty cylinders and predicts $Q_{\text{Pois}} = \pi R^4 P / (8\eta L)$. He assumed that, in a medium, the flow is possible only along non-intersecting thin channels, each of radius $R_c \ll R$, and the permeability can be identified as $\kappa \sim n^{\text{ch}} R_c^2$, with n^{ch} the number of open channels per unit surface [2].

This empirical law is valid not only for water flowing in sand but for all Newtonian fluids [3] embedded in a porous medium (namely a complex structure with strong heterogeneities such as soils, rocks or sand [4–7]). Indeed for such fluids n^{ch} is pressure-independent, as in each channel flow occurs for arbitrary weak pressure. This is not the case for another class of fluids, such as suspensions [8], gels [9], heavy oil [10], slurries or cement [11] for which a minimum yield stress σ_Y is needed to flow [12]. For these fluids n^{ch} grows with the applied pressure P . Experiments [13, 14] and numerical simulations [15–17] indicated that the Darcy law is indeed modified: below a threshold pressure P_0 no flow occurs while, above it, the flow grows non-linearly with P . Three flowing regimes are observed [18, 19]: i) initially the flow grows linearly in $P - P_0$ with a very small permeability $\sim 1/R^2$; ii) for larger pressure the flow grows non-linearly as $(P - P_0)^\beta$ (with $\beta \approx 2$) [20, 21]. iii) above a saturation pressure $P_{\text{sat}} \gg P_0$, the flow shows again a linear growth but with the much larger Newtonian permeability. Despite these

detailed observations, a theoretical explanation for the non-linearity is still lacking. In this letter we propose both an explanation and provide an explicit prediction for the modified Darcy law. We consider a porous structure with the geometry of a binary Cayley tree with t levels and 2^{t-1} channels (see Fig. 1). This geometry describes the flow in several biological networks (e.g. alveoli system in lungs [22] or leaf veins) and it is the simplest geometry with overlapping channels. Here we build on a method proposed in [23] to determine analytically n^{ch} as a function of pressure. Our model captures the three regimes of the flow, in particular the non-linear one is described by Eq. (13) and the saturation pressure reads $P_{\text{sat}} \sim P_0 + cst \cdot \ln t$. At this pressure there are $\sim t$ independent open channels and increasing further the pressure does not affect sensibly the permeability. The key point of our method is the identification of the first $\sim t$ open channels with the zero-overlap low energy states of the directed polymer on the Cayley tree, a model displaying one-step replica symmetry breaking (1-RSB) [24, 25]. Those low-overlap excitations are abundant in mean-field glassy disordered systems but their number is suppressed in finite dimension and their role in realistic set-ups is controversial. However, in the Darcy problem, excitations with high overlap are strongly penalized as they are inessential in increasing the flow independently of the spacial dimensionality. For this reason, low-overlap excitations play an important role also in finite dimension for the flow of yield stress fluids in porous media.

The model. — Our model is a Cayley tree pore network filled by a Bingham fluid described by the modified Poiseuille's law

$$Q_{\text{Pois}}(P) = \frac{\pi R^4}{8\eta L} (P - \tau)_+ \quad (2)$$

Here we denote $(x)_+ = \max(0, x)$ and $\tau = L\sigma_Y/R$ and consider $P > 0$. In this model large open pores are con-

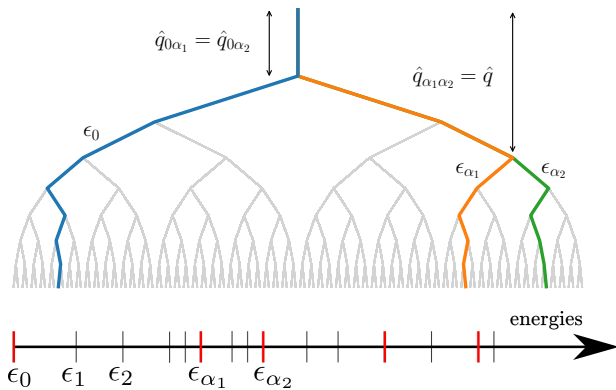


FIG. 1. Top: Binary Cayley tree with $t = 8$ levels. Each path α has an energy ϵ_α given by the sum of the thresholds along to the path. We assume a fixed pressure difference P between the top (root) and the leaves. Bottom: energies of the paths sorted as $\epsilon_0 < \epsilon_1 < \epsilon_2, \dots$. At the pressure $P_0 = \epsilon_0$ the channel indicated in blue opens. Increasing the pressure, the orange channel opens at pressure $P_1 > P_0$ (see (5)), the green one at pressure $P_2 > P_1$. The pairwise overlap are indicated in figure with \hat{q} the maximum among them. The energies corresponding to open channels are indicated in red in the axis at the bottom. In the large- t limit we show that $\hat{q} \ll t$ and $P_1 = \epsilon_{\alpha_1}, P_2 = \epsilon_{\alpha_2}, \dots$.

ected by tubes with random radius and unit length so that the threshold τ fluctuates from tube to tube. For simplicity we set to 1 the prefactor of (2) and we consider the Bingham rheology between two pores i and j as $Q_{ij} = (P_{ij} - \tau_{ij})_+$ with P_{ij} the pressure difference between the pores and the yield threshold τ_{ij} is drawn independently from a distribution $p(\tau)$. We are interested in determining the global flow function $Q_t(P; \tau)$ where τ represents the collective set of thresholds on each bond. Thank to the hierarchical structure, it is easy to obtain a recursive relation increasing the number of branches:

$$Q_t(P; \tau) = (P - P' - \tau_0)_+, \quad (3)$$

$$(P - P' - \tau_0)_+ = Q_{t-1}(P'; \tau^{(1)}) + Q_{t-1}(P'; \tau^{(2)}). \quad (4)$$

Eq. (3) comes from the constitutive relation applied on the topmost bond. Here P' is the pressure on the node connected to the root and τ_0 the corresponding threshold. The second relation descends from the conservation of the flow where $\tau^{(i)}$, $i = 1, 2$ are the sets of thresholds restricted to the two subtrees with $t - 1$ levels. Thus, assuming $Q_{t-1}(P; \tau)$ is known, one can use Eq. (4) to determine $P' = P'(P)$ and inject it in Eq. (3) to compute the flow function of the larger Cayley tree. Equations (3) and (4) are exact and amenable for numerical calculations, but their analytic treatment is possible only for vanishing thresholds, leading to the Newtonian behavior for $P > 0$, $Q_t(P) = \kappa_t^{\text{Newton}} P$, with the Newtonian permeability $\kappa_t^{\text{Newton}} = 2^{t-1}/(2^t - 1)$. To obtain analytical expression of the flow in the disordered case one has

to exploit the mapping with the directed polymer in the limit of large t .

Mapping to the directed polymer. — For each realisation of the thresholds τ , one has a sequence of pressures $\{P_0, P_1, P_2, \dots\}$ at which a new channel opens. As originally observed in [21], this sequence of pressures is also related to the energy levels of an associated directed polymer (DP) problem. Indeed, consider the directed paths on the Cayley tree connecting the root to the leaves. Interpreting the threshold τ_{ij} as the energy associated to the bond (ij) , we can associate an energy ϵ_α to each path α given by the sum of the thresholds belonging to the path. Ordering such energies as $\epsilon_0 < \epsilon_1 < \dots$, it is easy to verify that $P_0 = \epsilon_0$ (see figure 1). Moreover, since there is only one channel open, only one term in the right-hand side of Eq. (4) is non-vanishing and for $P \in [P_0, P_1]$, one gets simply $Q_t(P; \tau) = \frac{1}{t}(P - P_0)_+$. The computation of the flow for $P > P_0$ has a twofold difficulty: first, one needs to characterise the sequence of pressures P_1, P_2, \dots at which new channels open; second, for a given geometry of open channels, one needs to evaluate the effective permeability $\kappa \equiv dQ_t/dP$. Indeed for the subsequent channels, the relation between P_α involves not only the energies but also the overlaps (i.e. the number of common bonds) of the new channel with the previously open channels. For instance to open two channels one has to solve the following minimization

$$P_1 = \epsilon_0 + \min_{\alpha \neq 0} \frac{\epsilon_\alpha - \epsilon_0}{1 - \hat{q}_{0\alpha}/t} = \epsilon_0 + \frac{\epsilon_{\alpha_1} - \epsilon_0}{1 - \hat{q}_{0\alpha_1}/t} \quad (5)$$

where α_1 labels the path realising the minimum and $\hat{q}_{0\alpha}$ stands for the overlap between the α -th channel and the ground state. It is crucial to remark that in the minimization, among the low-energy excited states, the ones with high overlap with the ground state are strongly penalized by the factor $1/(1 - \hat{q}_{0\alpha}/t)$. The same property holds for the higher pressures P_2, P_3, \dots which display similar but more cumbersome dependence (see section A of [26]).

Large- t limit. — A major simplification occurs in the limit $t \rightarrow \infty$ as it is known that the directed polymers on Cayley tree display one-step replica symmetry breaking (1-RSB). For these systems the scaled overlap $q_{0\alpha} = \hat{q}_{0\alpha}/t$ converges, at large t , to a bimodal distribution, with either $q \rightarrow 0$ or $q \rightarrow 1$ [24] (finite t corrections are also known [27, 28]) implying $\hat{q}_{0\alpha} \sim 1$ or $\hat{q}_{0\alpha} \sim t$. Hence, in this large- t limit, among the two kinds of low-energy excited states, the open channels are of low-overlap type and basically uncorrelated. From this major simplification two other important properties arise: First, the opening pressures P_1, P_2, \dots coincide with the low energy levels $\epsilon_{\alpha_1}, \epsilon_{\alpha_2}, \dots$. Second, the total flow reduces to the sum of the contribution from each single open channel. As a consequence the computation of the flow problem reduces to determine the growth of the number of open channels n^{ch} as a function

of $x = P - P_0$. This number identifies with the number of low-energy excited states of the directed polymer, provided they have low overlap among them. We compute this number adapting the tools introduced in [23] and based on the mapping to the discrete Kolmogorov Petrovsky Piskunov (KPP) equation [25, 29–33].

KPP equation. — To begin, we introduce the number of states with energy smaller than $\epsilon_0 + x$, namely $m_t^{(\text{full})}(x) = \sum_{\alpha} \vartheta(x - (\epsilon_{\alpha} - \epsilon_0))$ ($\vartheta(x)$ is the Heaviside theta function). The statistics of $m_t^{(\text{full})}(x)$ was studied in [23] and its large- t behavior can be computed by making use of the mapping to the discrete KPP equation (see also section C of [26] for a summary). An important result is that the $t \rightarrow \infty$ limit exists finite, $m_{\infty}^{(\text{full})}(x) \equiv \lim_{t \rightarrow \infty} m_t^{(\text{full})}(x)$. The same result holds for the random energy model (REM) [24, 34], where the 2^t states are independent Gaussian random numbers of variance $\sigma^2 t$. In this case the average number of states is:

$$\overline{m_{\infty}^{(\text{REM})}}(x) = e^{\beta_c x} \quad (6)$$

with $\beta_c = \sqrt{2 \ln 2} / \sigma$ (the overline stands for the average over the disorder). For the DP a closed-form expression for the average number of states is not known [35]. Numerically it was shown in [23] that their number is larger than the corresponding REM model with the following asymptotics

$$\overline{m_{\infty}^{(\text{full})}}(x) \stackrel{x \gg 1}{\sim} A x e^{\beta_c x} \quad (7)$$

where A is an $O(1)$ non-universal constant. Here we are interested in a subset of states around the minimum, namely the number of open channels below the pressure $P_0 + x$, $n_t^{\text{ch}}(x) = \sum_a \vartheta(x - (P_a - P_0))$. Since one always has the upper bound $m_t^{(\text{full})}(x) > n_t^{\text{ch}}(x)$ the limit $n_{\infty}^{\text{ch}}(x) = \lim_{t \rightarrow \infty} n_t^{\text{ch}}(x)$ exists finite. It is tempting to identify their mean number $\overline{n_{\infty}^{\text{ch}}(x)}$ with the number of states of the corresponding REM $\sim e^{\beta_c x}$ [24], as the zero overlap states are basically uncorrelated paths.

A direct numerical investigation of this claim is possible only for moderate t and it is carried out by the exact flow problem using an algorithm derived from [21] and explained in section B of [26]. Our results are plotted in Fig. 3 left and display a slow convergence to our claim, but with strong finite size effects. To make progress we introduce the quantity $m_{\hat{q},t}(x)$ which counts, in a tree with t levels, the number of paths with energy $\epsilon_{\alpha} \leq P_0 + x$ and maximum overlap among themselves $\hat{q} = 1, \dots, t$. In practice, this can be obtained by a pruning procedure (see Fig. 2): at the level \hat{q} of the full Cayley tree, there are $2^{\hat{q}}$ subtrees labelled by $a = 1, \dots, 2^{\hat{q}}$. We replace each of these subtrees with a single bond with an effective energy that equals $\epsilon_0^{(a)}$, the minimal energy of the a -th subtree. These $2^{\hat{q}}$ remaining states correspond to the ones with maximal overlap \hat{q} . Clearly, for $\hat{q} = t$, we

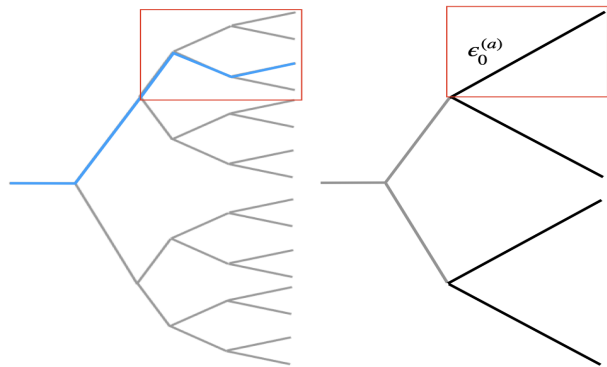


FIG. 2. Left: An example of Cayley tree with a total of $t = 5$ generations and 2^4 leaves. The minimal path of the topmost subbranch after $\hat{q} = 2$ generations is shown in bold. Right: Pruning of the full Cayley tree, where within each subtree starting from the \hat{q} -th generation, only the minimal path is retained.

recover $m_t^{(\text{full})}(x)$. If, on the contrary, we take first the limit $t \rightarrow \infty$, leading to $m_{\hat{q}}(x) = \lim_{t \rightarrow \infty} m_{\hat{q},t}(x)$, we are effectively considering energies with vanishing scaled overlap $\hat{q} \sigma_{\alpha} / t \rightarrow 0$. This remains true even if the limit $\hat{q} \rightarrow \infty$ is taken thereafter and we claim the following equality

$$n_{\infty}^{\text{ch}}(x) = \lim_{\hat{q} \rightarrow \infty} m_{\hat{q}}(x). \quad (8)$$

For $t \rightarrow \infty$ and finite \hat{q} , the pruning procedure is equivalent to growing a tree with \hat{q} levels where the leaves thresholds are drawn from the distribution of the minimum of an infinite tree. As a consequence, $\overline{m_{\hat{q}}(x)}$ can be computed by adapting the equations employed in [23] to compute $m_t^{(\text{full})}(x)$ as an integral of a function $r_t(x'; x)$:

$$\overline{m_t^{(\text{full})}}(x) = \int dx' r_t(x'; x) \quad (9a)$$

$$r_{t+1}(x'; x) = 2 \int d\tau p(\tau) \Omega_t(x' - \tau) r_t(x' - \tau; x) \quad (9b)$$

with initial conditions $r_1(x'; x) = p(x + x')$ and $\Omega'_1(x) = -p(x)$. Here $-\Omega'_t(x)$ is the distribution of the minimal energy of the directed polymer of t levels and it satisfies the discrete KPP equation:

$$\Omega_{t+1}(x) = \int d\tau p(\tau) \Omega_t(x - \tau)^2 \quad (10)$$

The recursive equations Eqs. (9) corresponds to growing a $t + 1$ -level tree starting from two t -level trees. Thus, to compute $\overline{m_{\hat{q}}(x)}$, one has to adjust the initial conditions (see section C.3 of [26]), starting from a single bond with a threshold drawn from the distribution of the minimum of an infinite tree $-w'_{\min}(x)$ [36]. Here $w_{\min}(x)$ solves the fixed point KPP equation

$$w_{\min}(x + c(\beta_c)) = \int d\tau p(\tau) w_{\min}^2(x - \tau) \quad (11)$$

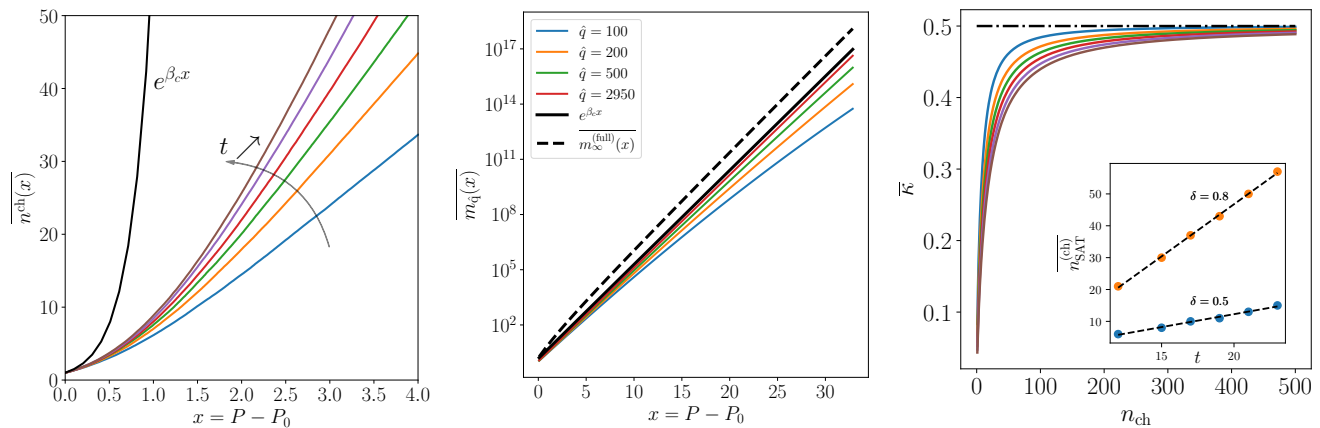


FIG. 3. Left: Exact numerical solution using the algorithm of section B of [26]. The threshold are Gaussian distributed with zero mean and variance $\sigma^2 = 1/12$. Hence $\beta_c = \sqrt{2 \ln 2}/\sigma$. Numerics is performed for moderate sizes $t = 12, 15, 17, 19, 21, 23$. The analytical prediction (solid line), valid when $t \rightarrow \infty$, is approached, but finite-size effects are still strong. Middle: $\overline{m_{\hat{q}}}(x)$ is obtained by numerical integration (section C of [26]) of Eqs. (9) starting from an initial threshold drawn from the fixed point distribution $-w'(x)$. $\overline{m_{\infty}^{(\text{full})}}(x)$ (dashed black line) is instead obtained for an initial threshold drawn from $\rho(t)$ and for $t = 10000$. Right: Average effective permeability $\overline{\kappa}$ for the data of Fig. 3 left. Only the first $\sim t$ channels are sufficient to reach an effective permeability close to the Newtonian one. Inset of right figure: t dependence of $n_{\text{SAT}}^{\text{ch}}$, defined as the average number of channels needed to saturate at the effective permeability $\delta \cdot \kappa_t^{\text{Newton}}$.

where $c(\beta_c)$ is the minimal value for which (11) has a solution (see section C.1 of [26]). Thus the equations for $\overline{m_{\hat{q}}}(x)$ are still equations (9) and (10) with the modified initial conditions $\Omega_{\hat{q}=1}(x) = w_{\min}(x)$ and $r_{\hat{q}=1}(x'; x) = -w'_{\min}(x + x')$. In Fig. 3 middle we compute numerically both $\overline{m_t^{(\text{full})}}(x)$ for large t and $\overline{m_{\hat{q}}}(x)$ for various \hat{q} . Their difference is clear, moreover we see that by increasing \hat{q} the solution approach the analytical prediction

$$\lim_{\hat{q} \rightarrow \infty} \overline{m_{\hat{q}}}(x) = e^{\beta_c x} \quad (12)$$

We refer to section D of [26] for an analytical derivation. We are now in the position of evaluating explicitly the average flow at large t . For a fixed $x = P - P_0$, there will be a finite number of open channels, sharing low overlap one with the other and each supporting a flow $(x - x')/t$, being $P_0 + x'$ its opening pressure. In this regime the total flow reduces the sum of the contribution from each single open channel, leading to

$$\overline{Q_t(P_0 + x)} \stackrel{t \rightarrow \infty}{=} \int_0^x \frac{dx'}{t} \overline{n_{\infty}^{\text{ch}}(x - x')} = \frac{e^{\beta_c x} - 1}{\beta_c t}. \quad (13)$$

Equation (13) is the main analytical result of the work and it is valid for moderate pressure above P_0 , describing both the linear single-channel as well as the non-linear behaviours observed in experiments.

Saturation pressure. — We now give an estimate for P_{sat} . Let us first observe that from Eq. (13), we obtain an exponentially growth in the permeability $\kappa_t = dQ_t/dP \sim e^{\beta_c(P - P_0)}/t$, however its value should saturate to $\kappa_t^{\text{Newton}} = 2^{t-1}/(2^t - 1)$. Equating the two regimes,

one obtains an saturation already at $P_{\text{sat}} - P_0 \sim \ln t/\beta_c$. Let us comment about this result: when the pressure is slightly above the minimal value P_0 , only a single channel os is open and the permeability is $\sim 1/t$. However, due to the fast growth of the density of available channels (12), a logarithmic increase in the pressure is enough to open $\sim t$ channels and saturate the permeability to its Newtonian value κ_t^{Newton} . A manifestation of this effect is shown in Fig. 3 right, where one observes the fast growth of the permeability followed by a negligible increase. Finally, in the inset of Fig. 3 right, we show the average number of channels $n_{\text{SAT}}^{\text{ch}}$ required for the permeability to surpass a certain fraction $\delta \cdot \kappa_t^{\text{Newton}}$ and the linear growth in t is apparent.

Conclusions. — In this work, we have presented the study of yield stress fluids on the Cayley tree. We show that the problem is closely related to the directed polymer in the same geometry. In particular, in the limit of large trees, a direct mapping emerges between n^{ch} and low-energy excited states with zero-overlap of the directed polymer. Thanks to this identification, we derive a simple universal expression for the flow as a function of the applied pressure. Equation (13) is independent of most microscopic details and threshold distribution and the tree branching ratio set only the parameter β_c .

The next big challenge would be to solve the problem of the flow in finite dimension. In particular it would be interesting to see if the low-overlap excitations of the associated directed polymer play a role also in the rheology of a finite dimensional porous medium.

Acknowledgements. — We thank X. Cao for discussions and suggestions. ADL acknowledges support by the ANR JCJC grant ANR-21-CE47-0003 (TamEnt). We acknowledge the support of the Simons foundation (grant No. 454941, S. Franz). This work was partly supported by the Research Council of Norway through its Center of Excellence funding scheme, project number 262644. Further support, also from the Research Council of Norway, was provided through its INTPART program, project number 309139. This work was also supported by "Investissements d'Avenir du LabEx" PALM (ANR-10-LABX0039-PALM).

-
- [1] H. Darcy, *Les fontaines publiques de la ville de Dijon: exposition et application...* (Victor Dalmont, 1856).
- [2] Indeed the total flow can be written as $Q = n^{\text{ch}} R^2 Q_{\text{Pois}}(R \rightarrow R_c)$ [37].
- [3] H. Barnes, *A handbook of elementary rheology* (University of Wales, Institute of Non-Newtonian Fluid Mechanics Aberystwyth, England, 2000).
- [4] J. Bear, *Dynamics of fluids in porous media* (Dover, 1988).
- [5] M. Sahimi, *Flow and transport in porous media and fractured rock: from classical methods to modern approaches* (Wiley, 2011).
- [6] M. J. Blunt, *Multiphase flow in permeable media* (Cambridge University Press, 2017).
- [7] J. Feder, E. G. Flekkøy, and A. Hansen, *Physics of flow in porous media* (Cambridge University Press, 2022).
- [8] A. Fall, F. m. c. Bertrand, G. Ovarlez, and D. Bonn, *Phys. Rev. Lett.* **103**, 178301 (2009).
- [9] J. Piau, *Journal of Non-Newtonian Fluid Mechanics* **144**, 1 (2007).
- [10] H. Pascal, *Acta Mechanica* **39**, 207 (1981).
- [11] P. Coussot, *Rheometry of pastes, suspensions, and granular materials: applications in industry and environment* (John Wiley and Sons, 2005).
- [12] E. Bingham, *Fluidity and Plasticity* (McGraw-Hill Book Company, New York, 1922).
- [13] T. Al-Fariss and K. L. Pinder, *Can. J. Chem. Eng.* **65**, 391 (1987).
- [14] G. Chase and P. Dachavijit, *Rheologica Acta* **44**, 495 (2005).
- [15] X. Lopez, P. H. Valvatne, and M. J. Blunt, *J. Colloid Interface Sci.* **264**, 256 (2003).
- [16] M. T. Balhoff and K. E. Thompson, *AIChE J.* **50**, 3034 (2004).
- [17] M. Chen, W. Rossen, and Y. C. Yortsos, *Chem. Eng. Sci.* **60**, 4183 (2005).
- [18] L. Talon and D. Bauer, *Eur. Phys. J. E* **36**, 139 (2013).
- [19] T. Chevalier and L. Talon, *Phys. Rev. E* **91**, 023011 (2015).
- [20] S. Roux and H. J. Herrmann, *Europhys. Lett.* **4**, 1227 (1987).
- [21] C. Liu, A. De Luca, A. Rosso, and L. Talon, *Phys. Rev. Lett.* **122**, 245502 (2019).
- [22] B. Mauroy, M. Filoche, E. R. Weibel, and B. Sapoval, *Nature* **427**, 633 (2004).
- [23] É. Brunet and B. Derrida, *Journal of Statistical Physics* **143**, 420 (2011).
- [24] M. Mézard, G. Parisi, and M. A. Virasoro, *Spin glass theory and beyond: An Introduction to the Replica Method and Its Applications*, Vol. 9 (World Scientific Publishing Company, 1987).
- [25] B. Derrida and H. Spohn, *Journal of Statistical Physics* **51**, 817 (1988).
- [26] See Supplemental material for additional information about: A) the derivation of few-channel solutions; B) the numerical implementation; C) the analytical approach based on the mapping onto the KPP equation; D) analytical derivation for the number of channels.
- [27] B. Derrida and P. Mottishaw, *EPL (Europhysics Letters)* **115**, 40005 (2016).
- [28] X. Cao, A. Rosso, R. Santachiara, and P. Le Doussal, *Phys. Rev. Lett.* **118**, 090601 (2017).
- [29] S. N. Majumdar and P. Krapivsky, *Physica A: Statistical Mechanics and its Applications* **318**, 161 (2003), sSTAT-PHYS - Kolkata IV.
- [30] S. N. Majumdar and P. L. Krapivsky, *Phys. Rev. E* **62**, 7735 (2000).
- [31] S. N. Majumdar and P. L. Krapivsky, *Phys. Rev. E* **65**, 036127 (2002).
- [32] L.-P. Arguin, A. Bovier, and N. Kistler, *Communications on Pure and Applied Mathematics* **64**, 1647 (2011).
- [33] K. Ramola, S. N. Majumdar, and G. Schehr, *Chaos, Solitons, Fractals* **74**, 79 (2015).
- [34] B. Derrida, *The random energy model*, Tech. Rep. (France, 1980) cEA-CONF-5131.
- [35] X. Cao, Y. V. Fyodorov, and P. L. Doussal, *SciPost Phys.* **1**, 011 (2016).
- [36] Note that the $w_{\min}(x)$ is defined up to an unimportant uniform shift in x as it is common to all the leaves of the pruned tree. Here we set the average minimum energy to zero.
- [37] F. A. Dullien, *Porous media: fluid transport and pore structure* (Academic press, 1991).
- [38] A. Kolmogorov, I. Petrovsky, and N. Piskunov, *Bull. Moscow State Univ. Ser. A: Math. Mech* **1**, 1 (1937).
- [39] M. Bramson, *Convergence of Solutions of the Kolmogorov Equation to Traveling Waves* (1983).

Supplementary Material

The Darcy's law of yield stress fluids on a tree-like network

Few-channel solution

In this section we report the derivation of the expression for P_1 used in the main text and P_2 . We also write down the expression of the flow for one and two channels. You can check that in the limit $t \rightarrow \infty$, $P_1 = \epsilon_{\alpha_1}$, $P_2 = \epsilon_{\alpha_2}$ and $tQ(P) = (P - P_0) + (P - P_1)$ for $P_0 < P < P_1$.

Flow for a single channel

At the critical pressure $P_0 = \epsilon_0$, corresponding to the ground state of the directed polymer, the first channels opens and the flow simply writes:

$$Q_{0,t}(P) = \frac{P - \epsilon_0}{t} \quad (1)$$

The subscript 0 indicates that only one channel (i.e. the ground state) is open. Such a formula holds for $P > P_0 = \epsilon_0$ but less than P_1 , the critical pressure at which a second channel opens. We will see in detail in the next section how it can be determined.

Explicit derivation flow up to two channels

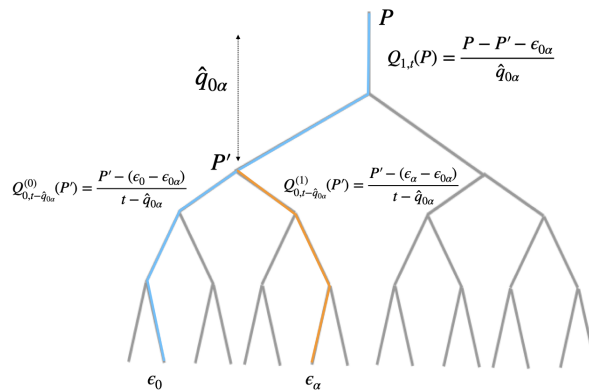


FIG. 4. Schematics for the Cayley tree with two open channels.

Let us now consider the case of a tree with two open channels (see figure 4). One is the ground state with energy ϵ_0 depicted in blue, the other is a channel with energy ϵ_α depicted in orange. These two channels have a common part of length $\hat{q}_{0\alpha}$ and we denote with $\epsilon_{0\alpha}$ the sum of the thresholds along this common portion. Along it, the fluid flows along a single channel with a pressure difference $= P - P'$, being P' the pressure at the bottom of the common part. We can thus write the flow adapting (1), upon replacing the length $t \rightarrow \hat{q}_{0\alpha}$, the energy $E_0 \rightarrow E_{0\alpha}$ and the pressure difference $P \rightarrow P - P'$. Given these ingredients, the flow reads:

$$Q_{1,t}(P) = \frac{P - P' - \epsilon_{0\alpha}}{\hat{q}_{0\alpha}} \quad (2)$$

The pressure P' can still be determined using the conservation of the flow, i.e. Eq. (4). Indeed:

$$\frac{P - P' - \epsilon_{0\alpha}}{\hat{q}_{0\alpha}} = Q_{0,t-\hat{q}_{0\alpha}}^{(0)}(P') + Q_{0,t-\hat{q}_{0\alpha}}^{(1)}(P') \quad (3)$$

where $Q_{0,t-\hat{q}_{0\alpha}}^{(0)}(P')$ is the flow along the subtree containing the ground state, $Q_{0,t-\hat{q}_{0\alpha}}^{(1)}(P')$ containing the other channel (see the two branches of figure 4). Since each of these is a single channel of length $t - \hat{q}_{0\alpha}$, we can use once again Eq. (1). One has

$$Q_{0,t-\hat{q}_{01}}^{(0)}(P') = \frac{P' - (\epsilon_0 - \epsilon_{0\alpha})}{t - \hat{q}_{0\alpha}}, \quad Q_{0,t-\hat{q}_{0\alpha}}^{(1)}(P') = \frac{P' - (\epsilon_\alpha - \epsilon_{0\alpha})}{t - \hat{q}_{0\alpha}} \quad (4)$$

From equation (3) we derive first the expression for $P'(P)$ and then $Q_{1,t}(P)$:

$$P'(P) = \frac{\hat{q}_{0\alpha}(\epsilon_0 + \epsilon_\alpha) + (t - \hat{q}_{0\alpha})P}{t + \hat{q}_{0\alpha}} - \epsilon_{0\alpha}, \quad Q_{1,t}(P) = \frac{2}{t + \hat{q}_{0\alpha}} \left(P - \frac{\epsilon_0 + \epsilon_\alpha}{2} \right) \quad (5)$$

Finally we impose the continuity of the flow $Q_{0,t}(\tilde{P}_1) = Q_{1,t}(\tilde{P}_1)$ to find the crossover pressure between one and two channels

$$\tilde{P}_1 = \epsilon_0 + \frac{t}{t - \hat{q}_{0\alpha}}(\epsilon_\alpha - \epsilon_0) \quad (6)$$

The criterion to select the first excited channel that opens above P_0 , is that the pressure P_1 is the smallest among all the \tilde{P}_1 computed for all possible two-channel geometries. This translates into

$$P_1 = \min_{\tilde{P}_1} \tilde{P}_1 = \epsilon_0 + \min_{\alpha \neq 0} \frac{t}{t - \hat{q}_{0\alpha}}(\epsilon_\alpha - \epsilon_0) \quad (7)$$

The channel satisfying the minimum condition is denoted by α_1 . As discussed in the main text, one sees from this expression that the minimization procedure involves a competition between the energy cost ϵ_α and the overlap $\hat{q}_{0\alpha}$.

In the next section, we show that a similar behavior holds even where three channels are open.

Expression of the flow for three channels

In this section, we report the behavior of the flow when three channels are open. There are three possible configurations for the position of the second excited channel with respect to the ground state and the first one. They each lead to a slightly different expression for the pressure P_2 , but all simplify to $P_2 = \epsilon_{\alpha_2}$ in the limit $t \rightarrow \infty$.

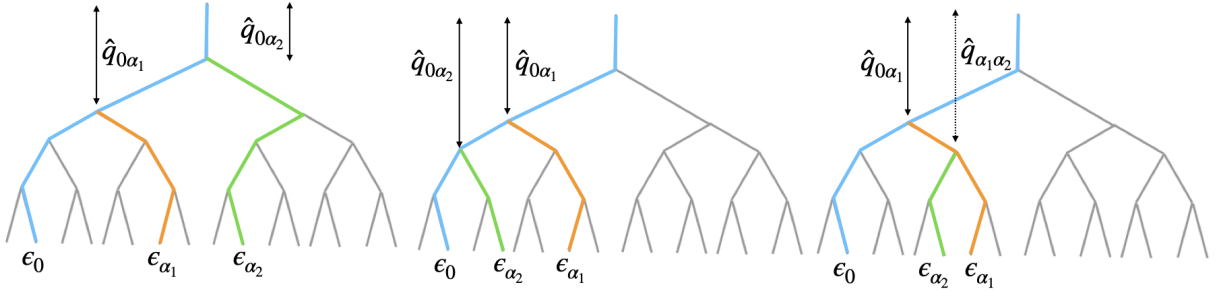


FIG. 5. Schematics for the Cayley tree with three open channels in the three possible geometrical arrangements.

Case I

The first case is the simplest: the second channel opens with a common overlap $\hat{q}_{0\alpha_2} = \hat{q}_{\alpha_1\alpha_2}$ with the ground state and the first channel. See figure 5 left. By construction, $\hat{q}_{0\alpha_2} < \hat{q}_{0\alpha_1}$.

The pressure P_2 reads:

$$P_2 = \min_{\alpha_2 \neq \{\alpha_1, 0\}} \left[\epsilon_{\alpha_2} - \frac{\hat{q}_{0\alpha_2}}{t + \hat{q}_{0\alpha_1} - 2\hat{q}_{0\alpha_2}}(\epsilon_{\alpha_1} + \epsilon_0 - 2\epsilon_{\alpha_2}) \right] \quad (8)$$

In the limit $t \rightarrow \infty$ we saw that $\hat{q}_{0\alpha_1} = O(1)$; from this and $\hat{q}_{02} < \hat{q}_{01}$, it follows that $\hat{q}_{02} = O(1)$ and $P_2 = \epsilon_{\alpha_2}$.

Case II

The second case corresponds to the opening of the second excited channel from the ground state with an overlap $\hat{q}_{0\alpha_2} > \hat{q}_{\alpha_1\alpha_2} = \hat{q}_{0\alpha_1}$. See figure 5 middle. The pressure P_2 reads:

$$P_2 = \epsilon_0 - \frac{\hat{q}_{0\alpha_1}}{t - \hat{q}_{0\alpha_1}}(\epsilon_{\alpha_1} - \epsilon_0) + \min_{\alpha_2 \neq \{\alpha_1, 0\}} \frac{t + \hat{q}_{0\alpha_1}}{t - \hat{q}_{0\alpha_2}}(\epsilon_{\alpha_2} - \epsilon_0) \quad (9)$$

When $t \rightarrow \infty$, the previous argument for the first excited channel sets $\hat{q}_{0\alpha_1}/t \approx 0$. In this limit, the resulting expression for P_2 is:

$$P_2 = \epsilon_0 + \min_{\alpha_2 \neq \{\alpha_1, 0\}} \frac{t}{t - \hat{q}_{0\alpha_2}}(\epsilon_{\alpha_2} - \epsilon_0) \quad \text{when } t \rightarrow \infty \quad (10)$$

This expression is identical to equation (7) with the substitution $\alpha \rightarrow \alpha_2$, and applying the same arguments of the first channel we arrive at setting $\hat{q}_{0\alpha_2}/t \approx 0$, leading $P_2 = \epsilon_{\alpha_2}$.

Case III

The last case is the mirror of the previous one, with the second channels that opens from the first one with overlap $\hat{q}_{\alpha_1\alpha_2} > \hat{q}_{0\alpha_1} = \hat{q}_{0\alpha_2}$. See figure 5 right. The pressure P_2 reads:

$$P_2 = \epsilon_0 + \frac{t}{t - \hat{q}_{0\alpha_1}}(\epsilon_{\alpha_1} - \epsilon_0) + \min_{\alpha_2 \neq \{\alpha_1, 0\}} \frac{t + \hat{q}_{0\alpha_1}}{t - \hat{q}_{\alpha_1\alpha_2}}(\epsilon_{\alpha_2} - \epsilon_{\alpha_1}) \quad (11)$$

When $t \rightarrow \infty$, the previous argument for the first excited channel sets $\hat{q}_{0\alpha_1}/t \approx 0$. In this limit, the resulting expression for P_2 is:

$$P_2 = \epsilon_1 + \min_{\alpha_2 \neq \{\alpha_1, 0\}} \frac{t}{t - \hat{q}_{\alpha_1\alpha_2}}(\epsilon_{\alpha_2} - \epsilon_{\alpha_1}) \quad \text{when } t \rightarrow \infty \quad (12)$$

This expression is again similar to equation (7) and applying the same arguments of the first channel we arrive at setting $\hat{q}_{\alpha_1\alpha_2}/t \approx 0$, leading $P_2 = \epsilon_{\alpha_2}$.

Exact numerical solution of the flow for the Cayley tree

The Darcy flow on the Cayley tree can be exactly numerically solved for moderate t and the code used in the paper is available [here](#). The solution consists in finding the pressures P_0, P_1, P_2, \dots at which each new channel opens. The

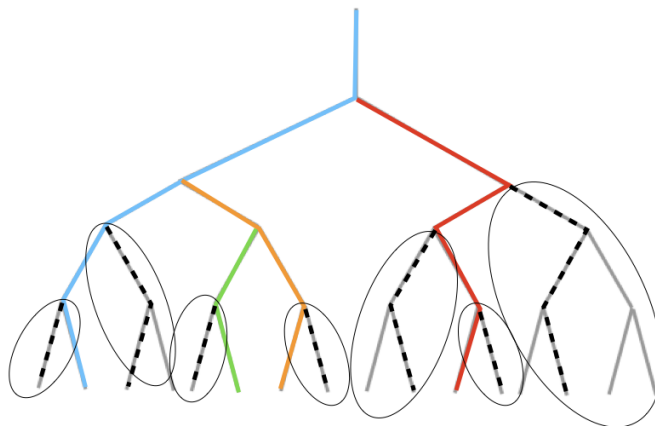


FIG. 6. Sketch of the algorithm used for the exact solution of the flow in the Cayley tree.

algorithm we use to produce the Fig. 3 left and the Fig. 3 right of the main text is a simplified version of the general

algorithm valid for any directed network and discussed in the supplementary material of [21]. In practice, the critical pressure P_0 is the ground state of the associated directed polymer model. The other pressures are found following an iterative procedure. At each step we denote by \mathcal{C}_s the subtree made of open channels exclusively for $P \in [P_s, P_{s+1}]$ (where P_{s+1} is not yet determined). Then,

1. Using Kirchhoff's equations, we determine the pressure at each node of \mathcal{C}_s as a function of the applied pressure P (these functions are linear in P).
2. We find all the subtrees connected to a node in \mathcal{C}_s which are still closed. In figure 6 they are highlighted by ovals.
3. For each subtree we find its ground state, denoted by $\mathcal{E}_s^{(1)}, \mathcal{E}_s^{(2)}, \dots$. They are indicated with dashed lines in figure 6.
4. We find the minimal applied pressure $\tilde{P}_s^{(1)}, \tilde{P}_s^{(2)}, \dots$ at which the ground state of each subtree opens. This is done by setting the node pressure at the root of each subtree (determined in step (1) using Kirchhoff's equation) equal to $\mathcal{E}_s^{(1)}, \mathcal{E}_s^{(2)}, \dots$.
5. We pick as a new channel the one with minimal opening pressure, namely $P_s = \min_\alpha \tilde{P}_s^{(\alpha)}$.

In numerical simulations we stop at $t = 23$ due to the exponential growth in t of the number of configurations on the Cayley tree.

Directed polymer on the Cayley tree: the KPP approach

The problem of a directed polymer on the Cayley tree can be studied using the formalism of the discrete KPP equation (see [23, 25] for the original literature). A binary Cayley tree of t levels has 2^{t-1} distinct paths denoted by α . Each path α has an associated energy given by the sum of the thresholds along the path:

$$\epsilon_\alpha = \sum_{i \in \alpha} \tau_i \quad (13)$$

Since any two paths α, α' have some bonds in common, the energies are correlated random variables. As a concrete example, for Gaussian thresholds $\tau_i \sim \mathcal{N}(0, \sigma^2)$, the correlation of the energies is given by

$$\overline{\epsilon_\alpha \epsilon_{\alpha'}} = \hat{q} \sigma^2 \quad (14)$$

where \hat{q} is the overlap between the two paths, namely the number of common bonds. The overbar indicates the average over the disorder.

A directed polymer on the Cayley tree with $t + 1$ levels can be constructed by considering two independent trees with t levels and joining them together by adding a bond with threshold τ . This hierarchical structure can be exploited when we want to study functions of the energies with a multiplicative form

$$G_t(x) = \overline{\prod_\alpha g(x - \epsilon_\alpha)} \quad (15)$$

for some $g(x)$. Indeed $G_{t+1}(x)$ and $G_t(x)$ can be related by the following discrete KPP recursive equation:

$$G_{t+1}(x) = \int d\tau p(\tau) G_t^2(x - \tau) \quad (16)$$

where $p(\tau)$ is the probability distribution of a single threshold and the initial conditions reads $G_{t=0}(x) = g(x)$.

A few relevant examples of functions $g(x)$ are:

- $g(x) = \theta(-x)$ (with $\theta(x)$ the Heaviside step function) used for the study of the minimum energy of the directed polymer. In particular we have

$$\Omega_t(x) = \overline{\prod_\alpha \theta(\epsilon_\alpha - x)} = \overline{\theta(\epsilon_0 - x)}, \quad \epsilon_0 = \min_\alpha \epsilon_\alpha \quad (17)$$

where $1 - \Omega_t(x)$ is the cumulative distribution of the minimum energy of a directed polymer of t levels.

- $g(x) = \lambda^{\theta(x)} = 1 + \theta(x)(\lambda - 1)$ for the study of the generating function $\Psi_t(x; \lambda)$ of $n_t(x)$, namely the number of states with energy smaller than x (see [23]):

$$\Psi_t(x; \lambda) = \overline{\lambda^{n_t(x)}}, \quad n_t(x) = \sum_{\alpha} \theta(x - \epsilon_{\alpha}) \quad (18)$$

In the following subsection we exploit these recursive KPP equations to describe various properties of the directed polymer on the Cayley tree which are relevant for the study of the Darcy law.

Discrete KPP equation

At large t , the discrete KPP equation (16) allows for travelling wave solutions of the form

$$G_t(x) = w(x + ct) \quad \text{when } t \rightarrow \infty \quad (19)$$

where c is the velocity of the traveling wave. When the initial conditions $G_0(x) = g(x)$ satisfy $\lim_{x \rightarrow \infty} g(x) = 0$ and $\lim_{x \rightarrow -\infty} g(x) = 1$, c is positive and the front moves backward (when the limits are reversed is c negative and the front propagates in the forward direction). The form of the front $w(x)$ satisfies the following fixed point equation:

$$w(x + c) = \int d\tau p(\tau) w^2(x - \tau) \quad (20)$$

We consider initial conditions of the form $g(x) \stackrel{x \rightarrow -\infty}{\approx} 1 - e^{\beta x}$. By substituting this form into equation (20) and expanding at first order in $e^{\beta x}$ one obtains an equation for c as a function of β :

$$c(\beta) = \frac{1}{\beta} \log 2 \int d\tau p(\tau) e^{-\beta \tau} \quad (21)$$

The velocity is shown, as a function of β , in figure () and presents a minimum at β_c . It was proven [29, 38, 39] that the increasing branch of $c(\beta)$ is unstable and that for $\beta > \beta_c$ both the velocity and the front shape freeze, namely $c(\beta > \beta_c) = c(\beta_c)$ and the front shape takes the form $w_{\min}(x)$ satisfying the fixed point equation:

$$w_{\min}(x + c(\beta_c)) = \int d\tau p(\tau) w_{\min}^2(x - \tau) \quad (22)$$

This equation corresponds to equation (11) of the main text.

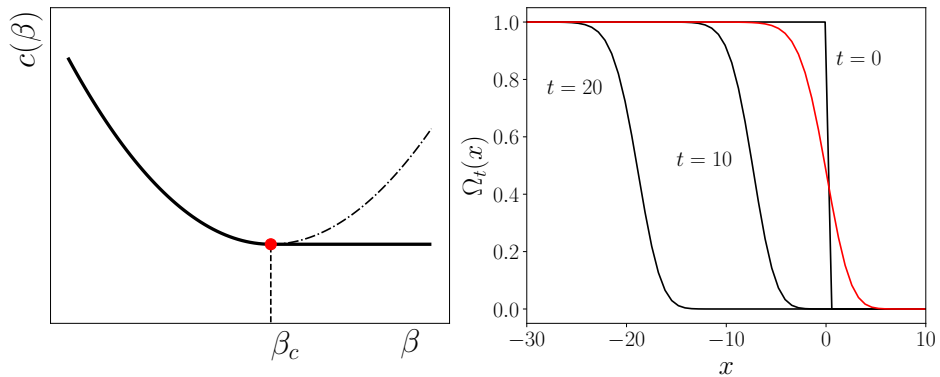


FIG. 7. Left panel: the dispersion relation of the velocity (black solid line) as a function of β . In the Gaussian case, $\tau \sim \mathcal{N}(0, \sigma^2)$, we find from equation (21) $c(\beta) = \ln 2/\beta + \beta\sigma^2/2$ with a minimum at $\beta_c = \sqrt{2 \ln 2}/\sigma$. For $\beta > \beta_c$ the value of the velocity freezes at $c(\beta_c)$. We report in dashed lines the unstable branch of $c(\beta)$ for $\beta > \beta_c$. Right panel: numerical solution for $\Omega_t(x)$ (17) for different values of t (black lines). At large t , $\Omega_t(x)$ approaches the stationary solution $w_{\min}(x)$ (red line), up to a t -dependent translation. Note that $w_{\min}(x)$ moves exactly at velocity $c(\beta_c)$ while the location of the front $\Omega_t(x)$ is $-c(\beta_c)t$ up to logarithmic corrections (23).

To study the minimum energy of the directed polymer the appropriate initial condition is $g(x) = \theta(-x)$ which corresponds to $\beta \rightarrow \infty$. Hence the directed polymer with minimal energy on a Cayley tree with t levels for large t is

$$P_0 = \epsilon_0 = -c(\beta_c)t + \frac{3}{2\beta_c} \log t + \chi_0 \quad (23)$$

The extensive part of the minimal energy, $-c(\beta_c)t$, comes from the velocity selection criterion. The subextensive logarithmic correction cannot be obtained by our first order analysis of equation (20) but was proven by Bramson [39]. The term χ_0 is a random variable of order 1 whose cumulative distribution is $1 - w_{\min}(x)$.

Average number of states above the minimum

Using the KPP formalism we can also study the number of states with an energy less or equal than x :

$$n_t(x) = \sum_{\alpha} \theta(x - \epsilon_{\alpha}) \quad (24)$$

Indeed by choosing as initial condition $g(x) = 1 + \theta(x)(\lambda - 1)$ we can obtain the generating function of $n_t(x)$, namely $\Psi_t(x) = \overline{\lambda^{n_t(x)}}$. However we are interested in the average number of states having an energy ϵ_{α} bigger than the minimal energy ϵ_0 of an amount x . We denote this quantity by:

$$m_t^{(\text{full})}(x) = \overline{\sum_{\alpha} \theta(x + \epsilon_0 - \epsilon_{\alpha})} = \overline{n_t(\epsilon_0 + x)} \quad (25)$$

This quantity is more complex than $n_t(x)$ since it involves the minimal energy ϵ_0 . However, following an approach introduced in [23], it is possible to derive an equation for $m_t^{(\text{full})}(x)$ that we can solve numerically. We sketch here the derivation. The reader uninterested to the technical details can skip directly to Eqs. (32,33).

The first step is to introduce the generating function of $m_t^{(\text{full})}(x)$ with $|\lambda| < 1$:

$$\chi_t(x; \lambda) = \overline{\lambda^{m_t^{(\text{full})}(x)}} \quad (26)$$

This function satisfies the following identity:

$$\chi_t(x; \lambda) = \int dx' \overline{\lambda^{n_t(x'+x)} \delta(x' - \epsilon_0)} = 1 + \partial_x \int dx' \overline{\lambda^{n_t(x'+x)} \theta(\epsilon_0 - x')} \quad (27)$$

To prove the validity of (27) we used $(\partial_x \lambda^n) \theta = (\partial_{x'} \lambda^n) \theta = \partial_{x'} (\lambda^n \theta) - \lambda^n (\partial_{x'} \theta)$. The integrand of equation (27) satisfies a discrete KPP equation (16) since it can be recast into a multiplicative form:

$$\lambda^{n_t(x'+x)} \theta(\epsilon_0 - x') = \prod_{\alpha} \lambda^{\theta(x'+x-\epsilon_{\alpha})} \theta(\epsilon_{\alpha} - x') \quad (28)$$

In this case the initial condition reads $g(x') = \lambda^{\theta(x'+x)} \theta(-x')$. The average number of states above the minimum can be written as:

$$\overline{m_t^{(\text{full})}(x)} = \partial_{\lambda} \chi_t(x; \lambda)|_{\lambda=1} \quad (29)$$

We thus expand for $\lambda = 1 - \varepsilon$

$$\overline{\lambda^{n_t(x'+x)} \theta(\epsilon_0 - x')} = \Omega_t(x') - \varepsilon R_t(x'; x) + O(\varepsilon^2) \quad (30)$$

The function $\Omega_t(x)$ is defined in (17). This expansion leads to:

$$\overline{m_t^{(\text{full})}(x)} = \int dx' \partial_z R_t(x'; x) = \int dx' r_t(x'; x) \quad (31)$$

where we set $r_t(x'; x) = \partial_x R_t(x'; x)$. Now, by plugging the expansion (30) in (16) and taking the first order in ε , we obtain a linear equation for $R_t(x'; x)$

$$R_{t+1}(x'; x) = 2 \int d\tau p(\tau) \Omega_t(x' - \tau) R_t(x' - \tau; x), \quad R_{t=0}(x'; x) = \frac{1}{2} \theta(x' + x) \theta(-x'). \quad (32)$$

Moreover because of the linearity of (32), $r_t(x; z)$ satisfies

$$r_{t+1}(x'; x) = 2 \int d\tau p(\tau) \Omega_t(x' - \tau) r_t(x' - \tau; x), \quad r_{t=0}(x'; x) = \frac{1}{2} \delta(x' + x) \quad (33)$$

By numerically solving simultaneously the equation for $\Omega_t(x)$ and (33), one has direct access to the t dependence of $\overline{m_t^{(\text{full})}}(x)$ (31).

Average number of states above the minimum with maximal overlap

In the main text we introduced the quantity $m_{\hat{q},t}(x)$ which counts the average number of states above the minimum with a maximal overlap \hat{q} . Simply by definition $\lim_{\hat{q} \rightarrow t} m_{\hat{q},t}(x) = m_t^{(\text{full})}(x)$. On the contrary, here we are interested in the limit $m_{\hat{q}}(x) = \lim_{t \rightarrow \infty} m_{\hat{q},t}(x)$. States of an infinite tree with maximal overlap \hat{q} can be built by first taking a tree of \hat{q} levels where the thresholds on each bond are distributed according to $p(\tau)$ and then adding the $\hat{q} + 1$ level with thresholds distributed according as $\chi_0 \sim -w'_{\min}(x)$. Indeed since we will be interested only in differences in energies we can use the distribution of fluctuations around the extensive part of the minimal energy. Then $m_{t=\hat{q}}^{(\text{full})}(x)$

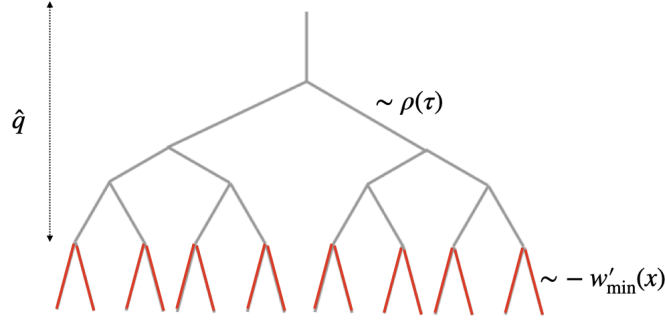


FIG. 8. Construction of the states with maximal overlap \hat{q} .

for this tree corresponds exactly to $m_{\hat{q}}(x)$ for an infinite tree. The only difference with respect to equations (32,33) is that term $\Omega_t(x)$ is replaced $w_{\min}(x + c(\beta_c)\hat{q})$. The equation (33) becomes:

$$r_{\hat{q}+1}(x'; x) = 2 \int d\tau p(\tau) w_{\min}(x' - \tau + c(\beta_c)\hat{q}) r_{\hat{q}}(x' - \tau; x) \quad (34)$$

Using $r_{\hat{q}}(x'; x)$ we obtain:

$$m_{\hat{q}}(x) = \int dx' r_{\hat{q}}(x'; x). \quad (35)$$

In the main text, in Figure 3 (middle panel), we show that $\overline{m_{\hat{q}}(x)}$ for large \hat{q} converges to $e^{\beta_c x}$ and is different from $\overline{m_t^{(\text{full})}}(x)$.

Numerical solutions

The directed numerical integration of $\Omega_t(x)$ (17) is not feasible at large t as the position of the front moves in the backward direction. In order to maintain the integration limits fixed in a window $[x_{\min}, x_{\max}]$ one needs to shift the front by fixing its position as t grows. Moreover to ensure a better numerical stability we evolve $H_t(x) = e^{-\beta_c x} (1 - \Omega_t(x))$ then the equation for (17) becomes:

$$H_{t+1}(x) = \int d\tau \tilde{p}(\tau) [2H_t(x - \tau) - e^{\beta_c(x-\tau)} H_t(x - \tau)] \quad (36)$$

with $\tilde{p}(\tau) = p(\tau)e^{-\beta_c\tau}$ and initial condition $H_0(x) = \theta(x)e^{-\beta_c x}$. To fix the position of $H_t(x)$ we compute numerically (Riemann sum) $b_t = \int dx H_t(x)e^{\beta_c x}$. At each step t if $b_t - b_0 > 0$ we make the substitution $H_t(x) \rightarrow H_t(x - (b_t - b_0))$. As we shift we should assign a value of $H_t(x)$ to the points in $[x_{\min}, x_{\min} + b_t - b_0]$; to do so interpolate the last 10 points using a spline. We employed $p(\tau) = \frac{1}{\sqrt{2\pi}}e^{-\tau^2/2}$ and discretized our integration limits $[x_{\min}, x_{\max}]$ in $N = 150000$ points with $x_{\min} = -10000$ and $x_{\max} = 30$. The equation for $r_t(x; z)$ (33) is solved in parallel to $H_t(x)$ taking into account the aforementioned translations. We use the same procedure to solve for $r_{\hat{q}}(x; z)$ (34).

Large \hat{q} limit of maximal overlap states

In the main text (12) we report the convergence of $\overline{m_{\hat{q}}(x)}$ to $e^{\beta_c x}$ as $\hat{q} \rightarrow \infty$. To get further insights about the large \hat{q} behavior of $\overline{m_{\hat{q}}(x)}$, we observe that Eq. (34) can be cast into the application of a \hat{q} -independent linear operator, by going in the co-moving frame. In other words, we introduce the shifted quantity $r_{\hat{q}}^{(s)}(x'; x) = r_{\hat{q}}(x' - c(\beta_c)\hat{q}; x)$. In this way, Eq. (34) becomes

$$r_{\hat{q}+1}^{(s)}(x'; x) = 2 \int d\tau p(\tau) w_{\min}(x' - \tau - c(\beta_c)) r_{\hat{q}}^{(s)}(x' - \tau - c(\beta_c); x) = [\mathcal{L} \cdot r_{\hat{q}}^{(s)}](x') = [\mathcal{L}^{\hat{q}} \cdot r_0^{(s)}](x') \quad (37)$$

where we implicitly defined the linear operator \mathcal{L} and in the last equality we iterated the linear equation to obtain a formal solution starting from the initial condition. The advantage of the formulation in terms of the shifted quantity $r_{\hat{q}}^{(s)}(x'; x)$ is that it involves a linear operator \mathcal{L} independent of \hat{q} . In the limit $\hat{q} \rightarrow \infty$, the operator \mathcal{L} acts as a projector on its largest eigenvector (assuming a gap is present). This can be easily identified taking the derivative of Eq. (22) with respect to x' , which shows

$$\rho_{\min}(x') = [\mathcal{L} \cdot \rho_{\min}(x')](x') \quad (38)$$

with $\rho_{\min}(x) = -w'_{\min}(x)$. In other words, the probability distribution function of the fluctuations around the minimum is an eigenvector. However, since the operator \mathcal{L} is not self-adjoint, in order to compute the projector on the eigenvector in (38), we need to determine the corresponding left eigenvector $\ell_{\min}(x)$. We introduce the standard scalar product between two functions $\ell(x)$ and $r(x)$ as

$$\langle \ell, r \rangle = \int dx \ell(x) r(x) \quad (39)$$

Then, $\ell_{\min}(x)$ must satisfy

$$\ell_{\min}(x) = [\mathcal{L}^\dagger \cdot \ell_{\min}](x) \quad (40)$$

where the adjoint of \mathcal{L} satisfies $\langle \ell, \mathcal{L} \cdot r \rangle = \langle \mathcal{L}^\dagger \cdot \ell, r \rangle$. In this way, we can formally express

$$\lim_{\hat{q} \rightarrow \infty} r_{\hat{q}}^{(s)}(x'; x) = \frac{\langle \ell_{\min}, r_0^{(s)} \rangle}{\langle \ell_{\min}, \rho_{\min} \rangle} \rho_{\min}(x') \quad (41)$$

Using (35), we can express the limit

$$\lim_{\hat{q} \rightarrow \infty} m_{\hat{q}}(x) = \frac{\langle \ell_{\min}, r_0^{(s)} \rangle}{\langle \ell_{\min}, \rho_{\min} \rangle} \int dx' \rho_{\min}(x') = \frac{\langle \ell_{\min}, r_0^{(s)} \rangle}{\langle \ell_{\min}, \rho_{\min} \rangle} \quad (42)$$

So the x -dependence is hidden in the scalar product in Eq. (42), which depends on $\ell_{\min}(x')$. Explicitly, the dual operator in Eq. (40) takes the form

$$[\mathcal{L}^\dagger \cdot \ell](x) = 2w_{\min}(x) \int dx' \ell(x') p(x' - x - c(\beta_c)) \quad (43)$$

The explicit form of $\ell_{\min}(x)$ cannot be determined in general as it depends on the specific form of the threshold distribution $p(\tau)$. So, it might look surprising that eventually the large \hat{q} drastically simplify to a universal form, but a subtle mechanism is at play. Indeed, in the limit $x \rightarrow -\infty$, we assume $\ell_{\min}(x) \sim e^{-\tilde{\beta}x}$. Plugging it in Eq. (40) and using that $w_{\min}(x \rightarrow -\infty) = 1$, we can determine the value of $\tilde{\beta}$. We obtain

$$2 \int dx' e^{-\tilde{\beta}x'} p(x' - x - c(\beta_c)) = e^{-\tilde{\beta}x} \quad (44)$$

and after the change of variables $\tau = x' - x - c(\beta_c)$, it coincides with Eq. (21) with $\tilde{\beta} = \beta_c$. Since $\rho_{\min}(x') \xrightarrow{x \rightarrow -\infty} x' e^{\beta_c x'}$ and $r_0^{(s)}(x'; x) = \rho_{\min}(x' + x)$, we see that both the numerator and denominator in Eq. (12) are formally infinite as the integrand have a finite limit for $x \rightarrow -\infty$. So the ratio in Eq. (42) needs to be evaluated by a limiting procedure. In order to regularize we introduce a cutoff Λ and set $\ell_{\min}^{(\Lambda)}(x) = \theta(x + \Lambda)\ell_{\min}(x)$. Then, we have

$$\lim_{\hat{q} \rightarrow \infty} m_{\hat{q}}(x) = \lim_{\Lambda \rightarrow \infty} \frac{\int_{-\Lambda}^{\infty} dx' \ell_{\min}(x') \rho_{\min}(x + x')}{\int_{-\Lambda}^{\infty} dx \ell_{\min}(x') \rho_{\min}(x')} = \lim_{\Lambda \rightarrow \infty} \frac{e^{\beta_c x} \int_{-\Lambda}^0 dx (x' + x) + O(1)}{\int_{-\Lambda}^0 dx' x' + O(1)} = e^{\beta_c x} \quad (45)$$

which gives the expected exponential behavior.

-
- [1] H. Darcy, *Les fontaines publiques de la ville de Dijon: exposition et application...* (Victor Dalmont, 1856).
- [2] Indeed the total flow can be written as $Q = n^{\text{ch}} R^2 Q_{\text{Pois}}(R \rightarrow R_c)$ [37].
- [3] H. Barnes, *A handbook of elementary rheology* (University of Wales, Institute of Non-Newtonian Fluid Mechanics Aberystwyth., England, 2000).
- [4] J. Bear, *Dynamics of fluids in porous media* (Dover, 1988).
- [5] M. Sahimi, *Flow and transport in porous media and fractured rock: from classical methods to modern approaches* (Wiley, 2011).
- [6] M. J. Blunt, *Multiphase flow in permeable media* (Cambridge University Press, 2017).
- [7] J. Feder, E. G. Flekkøy, and A. Hansen, *Physics of flow in porous media* (Cambridge University Press, 2022).
- [8] A. Fall, F. m. c. Bertrand, G. Ovarlez, and D. Bonn, *Phys. Rev. Lett.* **103**, 178301 (2009).
- [9] J. Piau, *Journal of Non-Newtonian Fluid Mechanics* **144**, 1 (2007).
- [10] H. Pascal, *Acta Mechanica* **39**, 207 (1981).
- [11] P. Coussot, *Rheometry of pastes, suspensions, and granular materials: applications in industry and environment* (John Wiley and Sons, 2005).
- [12] E. Bingham, *Fluidity and Plasticity* (McGraw-Hill Book Company, New York, 1922).
- [13] T. Al-Fariss and K. L. Pinder, *Can. J. Chem. Eng.* **65**, 391 (1987).
- [14] G. Chase and P. Dachavijit, *Rheologica Acta* **44**, 495 (2005).
- [15] X. Lopez, P. H. Valvatne, and M. J. Blunt, *J. Colloid Interface Sci.* **264**, 256 (2003).
- [16] M. T. Balhoff and K. E. Thompson, *AIChE J.* **50**, 3034 (2004).
- [17] M. Chen, W. Rossen, and Y. C. Yortsos, *Chem. Eng. Sci.* **60**, 4183 (2005).
- [18] L. Talon and D. Bauer, *Eur. Phys. J. E* **36**, 139 (2013).
- [19] T. Chevalier and L. Talon, *Phys. Rev. E* **91**, 023011 (2015).
- [20] S. Roux and H. J. Herrmann, *Europhys. Lett.* **4**, 1227 (1987).
- [21] C. Liu, A. De Luca, A. Rosso, and L. Talon, *Phys. Rev. Lett.* **122**, 245502 (2019).
- [22] B. Mauroy, M. Filoche, E. R. Weibel, and B. Sapoval, *Nature* **427**, 633 (2004).
- [23] É. Brunet and B. Derrida, *Journal of Statistical Physics* **143**, 420 (2011).
- [24] M. Mézard, G. Parisi, and M. A. Virasoro, *Spin glass theory and beyond: An Introduction to the Replica Method and Its Applications*, Vol. 9 (World Scientific Publishing Company, 1987).
- [25] B. Derrida and H. Spohn, *Journal of Statistical Physics* **51**, 817 (1988).
- [26] See Supplemental material for additional information about: A) the derivation of few-channel solutions; B) the numerical implementation; C) the analytical approach based on the mapping onto the KPP equation; D) analytical derivation for the number of channels.
- [27] B. Derrida and P. Mottishaw, *EPL (Europhysics Letters)* **115**, 40005 (2016).
- [28] X. Cao, A. Rosso, R. Santachiara, and P. Le Doussal, *Phys. Rev. Lett.* **118**, 090601 (2017).
- [29] S. N. Majumdar and P. Krapivsky, *Physica A: Statistical Mechanics and its Applications* **318**, 161 (2003), sTATPHYS - Kolkata IV.
- [30] S. N. Majumdar and P. L. Krapivsky, *Phys. Rev. E* **62**, 7735 (2000).
- [31] S. N. Majumdar and P. L. Krapivsky, *Phys. Rev. E* **65**, 036127 (2002).
- [32] L.-P. Arguin, A. Bovier, and N. Kistler, *Communications on Pure and Applied Mathematics* **64**, 1647 (2011).
- [33] K. Ramola, S. N. Majumdar, and G. Schehr, *Chaos, Solitons, Fractals* **74**, 79 (2015).
- [34] B. Derrida, *The random energy model*, Tech. Rep. (France, 1980) cEA-CONF-5131.
- [35] X. Cao, Y. V. Fyodorov, and P. L. Doussal, *SciPost Phys.* **1**, 011 (2016).
- [36] Note that the $w_{\min}(x)$ is defined up to an unimportant uniform shift in x as it is common to all the leaves of the pruned tree. Here we set the average minimum energy to zero.
- [37] F. A. Dullien, *Porous media: fluid transport and pore structure* (Academic press, 1991).
- [38] A. Kolmogorov, I. Petrovsky, and N. Piskunov, *Bull. Moscow State Univ. Ser. A: Math. Mech* **1**, 1 (1937).
- [39] M. Bramson, *Convergence of Solutions of the Kolmogorov Equation to Traveling Waves* (1983).